International Journal of Hydrogen Energy 199 (2026) 152753

Contents lists available at ScienceDirect

International Journal of Hydrogen Energy

journal homepage: www.elsevier.com/locate/he

Hydrogen isotope separation in "trapdoor" chabazite as measured by a novel sonic gas sensor

Lawrence Shere [a], Niklas Beere [a], Rosemary Brown [b], Rachel Lawless [b], Timothy J. Mays [a], Semali P. Perera [a], Alfred K. Hill [a,*]

[a] Department of Chemical Engineering, University of Bath, Bath, BA2 7AY, UK
[b] Culham Science Centre, Abingdon, OX14 3DB, UK

ARTICLE INFO

Keywords:
Chabazite zeolite
Hydrogen isotope separation
H_2 isotherm
Breakthrough testing
Trapdoor mechanism

ABSTRACT

Clean energy from nuclear fusion will require efficient technologies for hydrogen isotope separation. Separation by adsorption has shown high isotope selectivity, but only at impracticably low temperatures (<100 K). In this paper, the D_2/H_2 hydrogen isotope selectivity of 'trapdoor' chabazite is measured for the first time and compared to zeolite 5A, zeolite 3A, HKUST-1 and MOF-74(Ni). H_2 and D_2 isotherms for potassium chabazite show that between 143 and 195 K, H_2 adsorption is selectively blocked leading to high ideal isotope selectivity (D_2/H_2 = 1.83 at 143 K). Adsorption hysteresis is measured for the first time in trapdoor chabazite and zeolite 3A at similar temperatures which indicates trapdoor behaviour. An innovative breakthrough setup is developed including a whistle gas density sensor for deuterium detection. The D_2/H_2 separation factor of Na–K chabazite from frontal breakthrough is 2.71 at 159 K, which is much higher than for zeolite 5A at 1.25 at 159 K and 1.7 at 77 K.

1. Introduction

Fusion is expected to be an important future energy source, providing zero carbon energy generation [1,2]. However, a number of technical challenges need to be solved before fusion power generation can be commercialised. One of these is the requirement of a hydrogen isotope separation technology that must combine high separation efficiency, low energy intensity and low tritium inventory. Isotope separation is necessary to reprocess and maintain the 50:50 mixture ratio of deuterium (D_2) and tritium (T_2) fuel. Fusion reactors are expected to have a very low burn-up rate of roughly 2 %, necessitating recycling of the fuel [3,4]. For a proposed future power plant with 2 GW fusion power, 0.32 kg/day of tritium will be consumed [5] but due to the low burn-up rate, the recycled throughput will be 16 kg/day, which is almost 1000 times greater tritium throughput than required by the ITER fusion project currently under construction [3,6]. Cryogenic Distillation is commonly used for hydrogen isotope separation and has a moderate isotope selectivity (H_2/D_2 separation factor of 2.3 at 24 K [7]). However Cryogenic Distillation requires extremely low operating temperatures (20–24 K), which result in poor energy efficiency and has high tritium inventory in the liquid phase. As a result, no current technology meets the three key performance goals needed for future fusion energy plants.

In recent years, nanoporous adsorbents such as zeolites and metal-organic frameworks (MOFs) have been shown to have a high hydrogen isotope selectivity due to an effect known as Quantum Sieving (QS) [8]. Cu(I) open metal sites, such as Cu(I)-MFU-4l, have been reported to have one of highest heat of adsorption for hydrogen (32 kJ/mol) [9] leading to high D_2/H_2 selectivity of 11 at relatively high temperatures (100 K). Zhang et al. tested Ag-exchanged zeolite Y reporting a D_2/H_2 selectivity of 10 at a temperature of 90 K [10]. Among the adsorbents with lower heat of adsorption, Bezverkhyy et al. [11] recently reported a very high selectivity of 25.8 for chabazite zeolite at 38 K. All these adsorbents require extreme cryogenic operating temperatures (<100 K), and this will increase operation costs and complexity. The low temperature and high heat of adsorption would likely require the use of thermal desorption to fully regenerate the adsorbent after each adsorption cycle – a slow and energy intensive process. Therefore, an adsorbent that could operate at more mild temperatures with high hydrogen isotope selectivity would be more practical for tritium applications.

This paper reports the hydrogen isotope selectivity of chabazite (CHA) zeolite, which utilizes a molecular "trapdoor" mechanism to separate hydrogen isotopes. The "trapdoor" mechanism in CHA has so far been demonstrated to be able to distinguish non-polar gases such as

* Corresponding author.
E-mail address: a.k.hill@bath.ac.uk (A.K. Hill).

https://doi.org/10.1016/j.ijhydene.2025.152753
Received 17 July 2025; Received in revised form 29 October 2025; Accepted 22 November 2025
Available online 4 December 2025

N_2 and CH_4 with high selectivity [12]. The CHA framework contains large super-cavities accessed through narrow 8-membered ring (8 MR) apertures of 0.38 nm size as shown in Fig. 1 [13]. The 8 MR aperture is preferentially occupied by large cations such as K^+ which can control gas adsorption by acting as "gatekeeping" cations, also referred to as "trapdoor" cations. These gases demonstrate a critical admission temperature, below which the gas is blocked by the gatekeeping cation and adsorption is inhibited. Li et al. [14] measured the critical admission temperature for H_2 which was reported at approximately 170 K. Since the critical admission temperature is dependent on the gas type, by selecting a suitable temperature, the trapdoor effect can block one gas type while allowing another to adsorb. If the critical admission temperature is different for H_2 and D_2, the trapdoor effect could be used to separate hydrogen isotopes at temperatures much higher than other adsorbents. There are no reported D_2 adsorption isotherms or quantitative separation data for hydrogen isotopes using trapdoor CHA, but a possible isotope selectivity is indicated by two previous studies. Physick et al. [15] tested caesium exchanged CHA at 293 K using a column breakthrough setup, reporting an isotope selectivity but did not provide quantitative adsorption data. Taguchi et al. [16] tested potassium exchanged CHA using Thermal Adsorption Spectroscopy reporting an isotope selectivity occurring at around 200 K. However, the separation factor was not reported and the stated H_2 uptake was very low.

In this work, H_2 and D_2 isotherm measurements are conducted between 77 and 273 K to find the critical admission temperature of H_2 and D_2 of K exchanged CHA (K-CHA). These isotherm measurements provide understanding of the adsorption equilibria and are an important first step in understanding the selectivity of an adsorbent. A thorough comparison of the selectivity performance of the trapdoor effect is made by testing other high-performance adsorbents including zeolite 5A, 3A, MOF-74(Ni) and HKUST-1. MOF-74(Ni) and HKUST-1 are MOFs that have potential for hydrogen isotope separation due to the presence of open metal sites [17]. Zeolite 5A has been shown to be effective for hydrogen isotope separation at 77 K [18] but has not yet been tested at higher temperatures (159 K). Zeolite 3A shows remarkable similarities to trapdoor K-CHA since it contains K^+ cations which have been shown to restrict H_2 adsorption at cryogenic temperatures (<160 K) [19]. In this study, H_2 and D_2 admission of zeolite 3A and 5A are measured between 143 and 195 K and directly compared to the trapdoor mechanism of K-CHA. Breakthrough experiments using mixed D_2/H_2 are then used directly to measure the D_2/H_2 selectivity of NaK-CHA under dynamic adsorption conditions.

Normally, mass spectrometry is required for D_2/H_2 breakthrough testing to provide real time isotope measurements but it is expensive. In this work, a simple sonic gas detector using a miniaturised whistle was developed and used successfully to conduct breakthrough testing. Sonic detectors have been used for other gases [20,21] but this is the first test of a whistle type detector for analysing hydrogen isotopes. The whistle detector showed some limitations with the minimum gas flow, but these results show that it is a cost-effective alternative to conventional mass spectrometry for isotope measurements, enabling additional research into this important area for fusion energy.

2. Method

Copper nitrate trihydrate (ACS reagent, >97 %), nickel acetate tetrahydrate (purum p.a., >99 %), potassium hydroxide pellets (ACS reagent), trimesic acid (>95 %, benzene-1,3,5-tricarboxylic acid (BTC)), formic acid (ACS reagent, >95 %), hydroquinone (reagent plus, >99 %), potassium carbonate (ACS reagent, >99 %), 37 % hydrochloric acid, sodium sulfite (Na_2SO_3, ACS reagent, >98 %) were purchased from Merck and used as supplied.

Zeolite 5A powder was purchased from Molsiv Adsorbents, UOP and used as purchased. Zeolite 5A, 1.56 mm pellets were purchased from BDG Chemicals Ltd, Poole, UK and used as supplied. Reagent grade KCl and NaCl were purchased from Sigma Aldrich. Wyoming sodium bentonite was purchased from RS Minerals, UK. Ethanol (>99%), acetone (>99%) and n-pentane (>99%) were purchased from VWR and used as supplied.

2.1. Adsorbent synthesis

Chabazite (CHA) was synthesised from Zeolite Y material using a standard procedure adapted from Gaffney [173] (full method for all adsorbent synthesis is given in the supporting information). MOF-74(Ni) was synthesised based on an aqueous reflux method by Cadot et al. [22] and adapted to achieve higher purity. HKUST-1 was synthesised under solvothermal conditions using a standard method in the literature [23]. NaK-CHA pellets were prepared using 15 wt.% bentonite clay as the binder. A soft paste was formed by adding water and then was extruded through a 2 mm syringe to form pellets. The pellets were fired at 600 °C and ion exchanged using a mixed solution of NaCl and KCl.

2.2. Powder X-ray diffraction (P-XRD)

Powder X-ray Diffraction (P-XRD) was conducted on all samples to identify the presence of high purity crystalline phases. The STOE STADI P system accessed through the Material and Chemical Characterisation

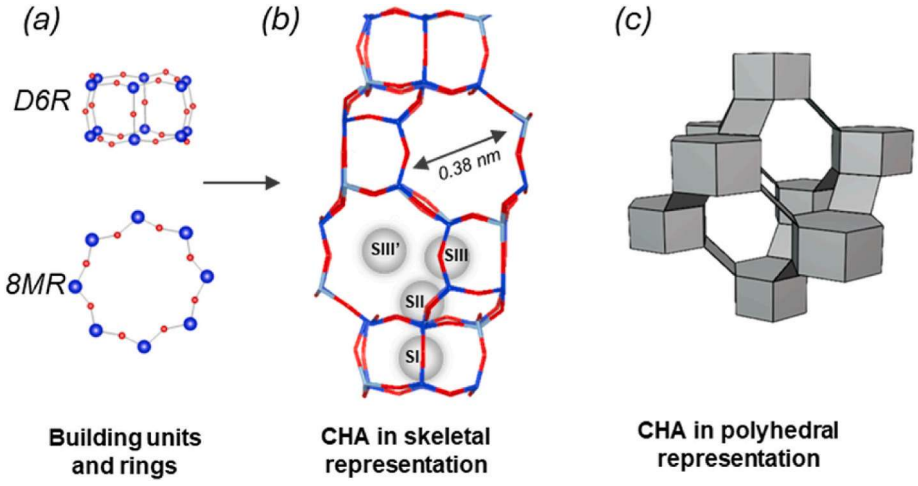

Fig. 1. (a) Building units and rings for chabazite (CHA) zeolite: (b) Framework structure and assignment of cation positions for CHA. SIII' position in the 8-membered ring (8 MR) is favoured by large cations (K^+) which then act as trapdoor cations. (c) Polyhedral representation of CHA highlighting passages available to gas molecules (H_2O or larger, including H_2 and D_2) and the CHA super-cavity accessed through the 8 MRs.

(MC2) laboratory located at the University of Bath was used. The system is equipped with a Multi-Mythen moving detector and a germanium primary beam monochromator operating in transmission mode using CuKα1 radiation (λ = 1.54051 Å).

2.3. Energy-dispersive X-ray spectroscopy (EDX)

An Oxford instruments ULTIM max 170 and 10 kV acceleration voltage was used, which was accessed through the Material and Chemical Characterisation (MC2) laboratory located at the University of Bath. The powder sample was deposited on carbon tape, and five areas of the sample of roughly 100 μm size were analysed.

2.4. Adsorption isotherms

A Micromeritics 3Flex instrument was used to conduct adsorption and partial desorption isotherms using either H_2, D_2 or N_2. Samples were initially degassed under N_2 flow for 1 h at 90 °C, then 1 h at the final degas temperature. The samples were then degassed under vacuum for 8 h at the final degas temperature. The final degas temperature for all adsorbents was 350 °C except for HKUST-1 (200 °C) and MOF-74(Ni) (slowly ramped over 1 h to 250 °C). The free space of the sample tube was minimised using a glass filler rod (the same rod in each test) and the free space was directly measured with helium at the end of each experiment.

During the isotherm measurement, standard temperatures were maintained using liquid nitrogen (77 K) or water ice bath (273 K). Other non-standard isotherm temperatures were achieved using solvent liquid/ice cooling baths which maintain a stable temperature at the melting point of the solvent (pentane: 143 K, ethanol: 159 K, acetone: 178 K, acetone/dry ice: 195 K). Normally solvent ice will tend to sink to the bottom and so not cool the solvent at the top. If the container can be fully packed with solvent ice, then this is not an issue. However, the sample tube needed space to be safely lowered, so an alternative setup was required. A novel setup using a hanging solvent ice container (or dry ice pellets in an open mesh cage) was used. The container was suspended in the Dewar next to the sample tube keeping the ice separate (see Fig. 2). A custom-built stainless steel cylindrical mesh cage (30 mm OD, 200 mm high) wrapped in aluminium foil was used as the container. The container is filled with solvent and frozen in liquid nitrogen before suspending in the Dewar containing pre-cooled solvent. This setup provides several advantages over a standard solvent ice bath for isotherm adsorption measurement. Since the frozen solvent is suspended, the solvent at the top is efficiently cooled and will produce natural convection currents preventing hot spots forming. Large amounts of solvent ice can be used providing cooling for longer experiments, while leaving ample space for the sample tube to be safely lowered/raised during automatic operation. Using this setup, many different cryogenic isothermal temperatures could be reached which would normally require a specialised cryostat attachment. The temperature was measured using a thermocouple at several points in the Dewar and was found to remain within 5 K of the solvent freezing point during a 3 h isotherm experiment.

BET surface area was calculated from N_2 isotherms conducted at 77 K. The BET model was fitted to 5 pressure data points in a pressure range for which the value of v_{ads} (1- P/P_0) was always increasing with P/P_0 [24].

Ideal Adsorbed Solution Theory (IAST) was used to calculate the ideal selectivity from the individual H_2 and D_2 isotherms at 77 K. For the high temperature isotherms (143–273 K), the isotherm shape is close to linear and so the D_2/H_2 adsorption ratio was used directly as the ideal selectivity.

2.5. Breakthrough rig design and dynamic H_2/D_2 adsorption testing

The breakthrough rig schematic is shown in Fig. 3. Flow rates of between 35.5 and 336 ml_n/min were used with D_2 concentrations between 5 and 28.6 vol.%. Flow rates are reported under normal reference conditions (reference gas volumetric flow at 273 K and 101.3 kPa with gas molar volume of 22.4 ml_n/mmol). The adsorption column was U-shaped with an inner diameter of 10 mm and 300 mm length. See supporting information for further details of column, piping and gas flow controllers.

The adsorbents tested using the breakthrough rig were NaK-CHA at 159 K and zeolite 5A at either 77 K or 159 K with the adsorbent mass and measured column free space shown in Table 1. The adsorbent samples were degassed in-situ firstly under H_2 flow (60 ml_n/min), with the temperature slowly increased to 90 °C and held for 2 h. The column was

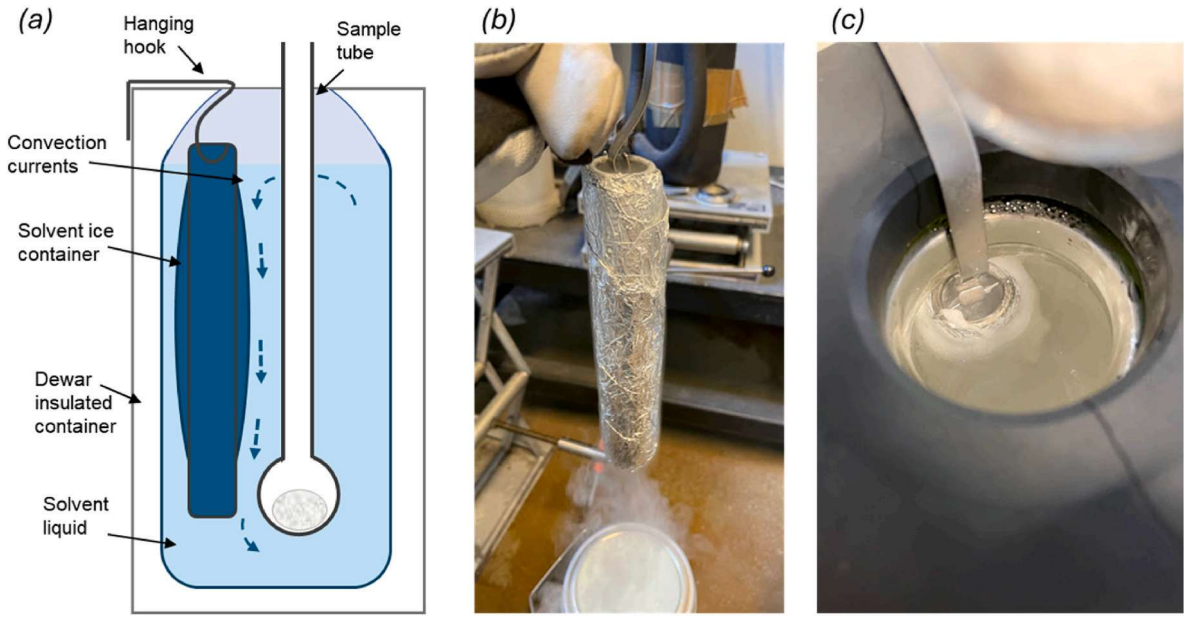

Fig. 2. (a) Novel setup of solvent cooling bath used to maintain temperatures at the solvent melting point for adsorption isotherms. (b) The solvent was frozen in a hanging container using liquid nitrogen forming a solid icicle which was suspended in the Dewar, shown in (c). This provides a convenient method of introducing a large amount of solvent ice which kept the Dewar cool while keeping it separate from the sample tube.

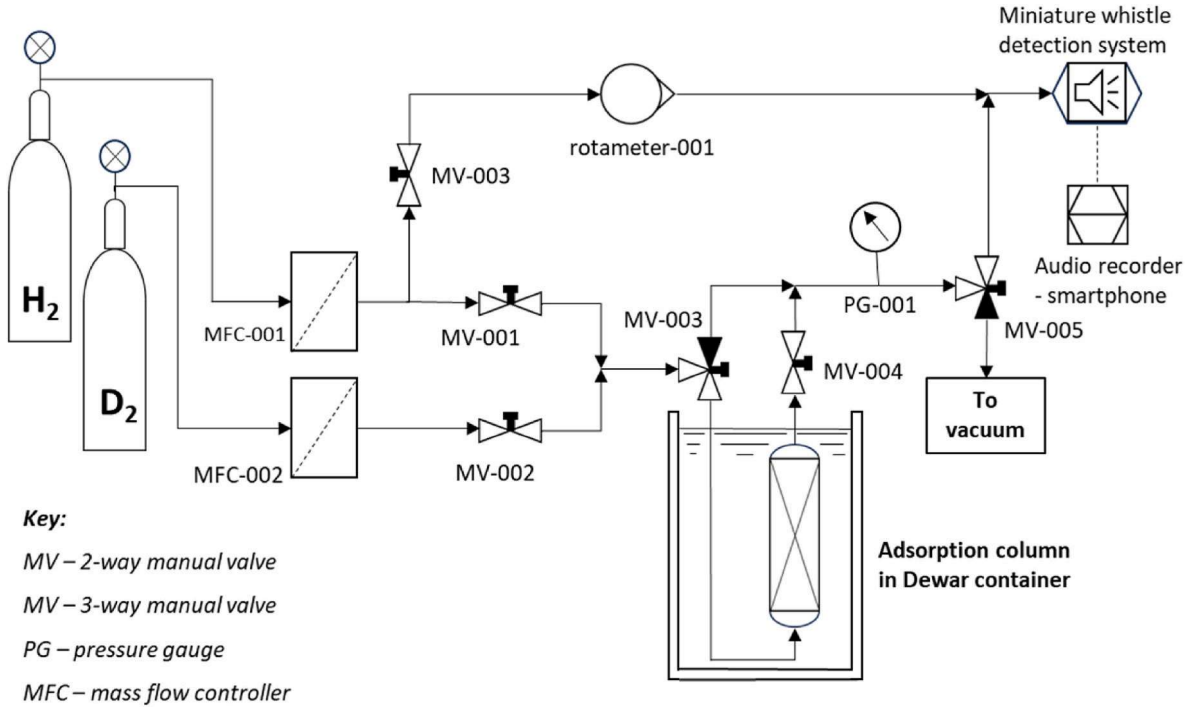

Fig. 3. Schematic of breakthrough rig which was designed and constructed for use in dynamic D_2/H_2 adsorption tests using displacement and frontal modes.

Table 1
Adsorbent mass and system free volume. Free space volume was measured at 293 K using H_2, then calculated for analysis temperature.

Sample	Analysis Temp (K)	Adsorbent mass (g)	Calculated Free Space Volume (ml_n)
Zeolite 5A	77	14.7	**85.5**
Zeolite 5A	159	14.7	**45.1**
NaK-CHA	159	5.9	**43.2**

then held under vacuum using a diaphragm pump with H_2 flow continued. The column was heated to 350 °C and kept at this temperature for 8 h.

The adsorbents were tested using two different breakthrough experiments: displacement and frontal breakthrough. For the displacement mode breakthrough test, the adsorption column was firstly saturated with H_2 at 1 bar. The H_2 flow was then switched to mixed D_2/H_2 flow and the time taken for the D_2 to reach the column outlet was measured. In the frontal mode breakthrough test, the adsorption column was initially at vacuum pressure with the outlet closed. A flow of mixed D_2/H_2 was introduced at the column inlet to pressurise the column. Once the pressure reaches 1 bar, the outlet was opened, and the time taken for the D_2 to reach the column outlet was measured. The full breakthrough method is given in the supporting information.

2.6. Real-time gas analysis using a bespoke online whistle gas density sensor

A novel approach for analysing hydrogen isotope composition using a whistle gas density sensor was developed and successfully used for breakthrough tests. The different speed of sound in H_2 and D_2 causes a change in the sound frequency of a whistle. The whistle was miniaturised, reducing the minimum H_2 flow rate required to produce a stable sound to 336 ml_n/min.

When the flow to the bed is necessarily lower, the hydrogen flow was partially bypassed around the bed to maintain the minimum flow to the sensor. In these cases, the D_2 concentration into the bed was increased to maintain the minimum D_2 concentration to the whistle when diluted with the bypassing hydrogen. For these reasons, both the flow rate through the bed and the D_2 concentration to the bed had to be varied depending on the adsorbent and its anticipated uptake.

The whistle was constructed of a brass tube with an inner diameter of 1.57 mm and total length of 22 mm (15 mm length from edge to back stop). A v-shaped opening was made in the brass tube, just beyond the opening shown in Fig. 4(a & c). A narrowing in the opening is made by filing a flat edge on a brass rod and this is glued in place (see Fig. 4(b)) along with a back stop to close the end of the tube.

2.7. Breakthrough calculations

The D_2/H_2 separation factor $S(D_2/H_2)$, was calculated from area (A) and area (B) in the frontal breakthrough results, as shown in Fig. 5 [25] and the flow rate, Q. During the initial phase of the experiment (area A), the outlet valve is closed and so the column accumulation is equal to the input flow. Once the column is pressurised, the outlet is opened and the output D_2 concentration is measured (area B). It was assumed that the outlet flow rate is equal to the inlet flow, once the column outlet is opened.

$$A\ (ml_n/(\mathrm{g\ min})) = A\ (s) \times Q\left(\frac{ml_n/(\mathrm{g\ min})}{60\ (s/\mathrm{min})} - FSV\ (ml_n/g)\right) \quad (1)$$

$$B\ (ml_n/(\mathrm{g\ min})) = \frac{B\ (s) \times Q\ (ml_n/(\mathrm{g\ min}))}{60\ (s/\mathrm{min})} \quad (2)$$

The separation factor was calculated using equation (3):

$$S(D_2/H_2) = \frac{(A+B)}{A} \quad (3)$$

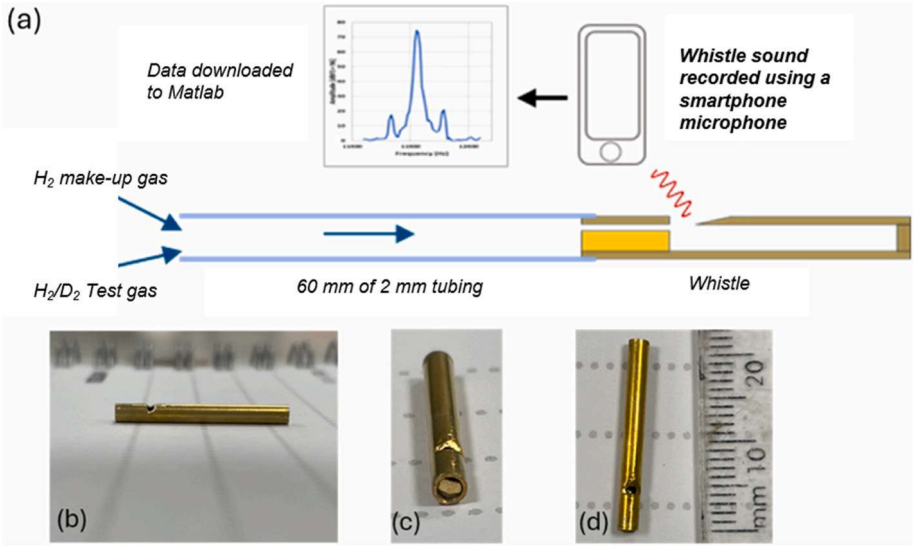

Fig. 4. (a) Sonic detection system using a miniaturised whistle to detect changes in the gas density. The whistle required additional gas flow which was provided by a H_2 make-gas line. (b–d) Photos of the whistle used to analyse the hydrogen isotope mixture. The gas flow enters through a narrowing in the front (shown in (c)) towards a sharp edge formed by a groove cut in the side. This causes the gas flow to become unstable and start to oscillate. The resonant frequency of these oscillations is directly proportional to the speed of sound in the gas making it sensitive to the hydrogen isotope composition.

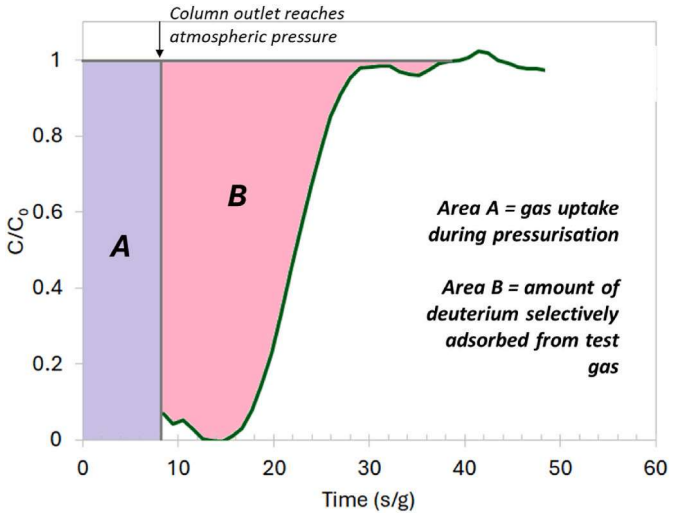

Fig. 5. Analysis of frontal mode breakthrough curve. Initially the mixed H_2/D_2 feed is adsorbing to the packing at vacuum pressures with the outlet closed (area A). Next, once the column has reached atmospheric pressure, the outlet is opened and the D_2 concentration is measured. Using areas (A) and (B) the $H_2 + D_2$ uptake, and D_2/H_2 separation factor were calculated. Note the breakthrough plot begins above zero. This is because at the beginning, the flow out of the column is lower due to adsorption, and this causes a small reduction in the frequency of the whistle gas density sensor.

The uptake of D_2 and H_2 is calculated from areas *A* and *B* as follows:

$$uptake\ of\ D_2(ml_n/g) = y_D(A + B) \tag{4}$$

$$uptake\ of\ H_2(ml_n/g) = Ay_H \tag{5}$$

where y_D and y_H are the fractions of D_2 and H_2 in the feed gas respectively ($y_D + y_H = 1$). The D_2 uptake for displacement breakthrough was calculated in the same way.

The raw signal data was sampled every 3 s, and a moving average was applied to remove noise. Three potential sources of error from each breakthrough experiment were analysed: the error in free space correction was found to have negligible impact, manual operation/timing errors contributed 5–8 %, and error in supply flow rate contributed 5–15 %, largely due to the rotameter instrument, and the combined error was 10–40 % depending on the flowrate. The full error analysis is given in the supporting information.

The system free space comprises the empty volume present in the pipes, fittings and the column. The warm free space volume was measured using H_2 at ambient temperatures (293 K). The free space at the experimental temperature can be estimated assuming ideal gas behaviour shown in equation (6).

$$Free\ Space\ Volume = Warm\ column\ volume \times \frac{T_{warm}}{T_{cold}} + Volume\ of\ pipework \tag{6}$$

3. Results and discussion

3.1. Material characterisation

Synthesised K-CHA was tested using powder XRD to confirm that the crystal structure of CHA had been produced and that there was no zeolite Y precursor remaining in the sample. Theoretical XRD peaks for CHA occur at $2\theta = 9.5, 13, 16, 18, 20.5^\circ$ while for the zeolite Y precursor they are found at $2\theta = 6.2, 10, 12, 15.5, 19^\circ$ [26] (see supporting information for XRD pattern of K-CHA, MOF(Ni) and HKUST-1). The XRD pattern shows the expected CHA peaks from the theoretical CHA pattern with none of the peaks from Zeolite Y, showing full conversion and a successful synthesis. Some of the K-CHA peaks are slightly shifted and/or wider than the theoretical peaks. Peak broadening is caused by the smaller crystal sizes [13]. The presence of adsorbed water and Al atoms in the framework will shift the peak positions and so will not perfectly conform to the theoretical peaks [13].

The EDX results showed the K-CHA sample had a Si/Al ratio of 1.98 with a K cation content of 97.6 mol.% with the remainder being Na (see Table 2). A N_2 isotherm was conducted at 77 K and the BET surface area was calculated to be 29 m^2/g. This extremely low BET surface area indicates that at the low temperature of 77 K, N_2 is blocked from the pores indicating the presence of a "trapdoor" that is closed for N_2 at 77 K [27]. For MOF-74(Ni) the BET surface area was measured to be 1365–1495 m^2/g and for HKUST-1 it was 1663–2045 m^2/g indicating high porosity samples have been successfully prepared [23,28–31]. The N_2 isotherms at 77 K for K-CHA, MOF-74(Ni) and HKUST-1 are shown in the

Table 2
Summary of EDX results from testing K-CHA and two ion exchanged CHA samples.

Sample	Ion exchange (mol%)	Cations detected	Si/Al ratio	Cation/Al ratio
K-CHA	97.6 ± 0.4	K, Na	1.98 ± 0.05	1.01 ± 0.10
K-CHA(IE)	98.5 ± 0.01	K, Na	1.92 ± 0.02	0.94 ± 0.08
NaK-CHA	81.8 ± 0.01	K, Na	2.06 ± 0.01	1.01 ± 0.04

supporting information.

3.2. Effect of temperature on H_2 & D_2 adsorption to K-CHA

H_2 and D_2 isotherms were measured for K-CHA at different temperatures between 77 K and 273 K. The amount of H_2 and D_2 adsorbed at 100 kPa for each temperature and the ideal D_2/H_2 selectivity was calculated and is shown in Fig. 6 alongside the isotherms. Above 195 K, the uptake of H_2 and D_2 is almost the same showing negligible selectivity. As the temperature is reduced from 273 K, adsorption uptake initially increases as is expected for exothermic adsorption, but between 195 K and 143 K, the adsorption begins to be blocked and reaches a maximum at 159 K. Between 159 K and 143 K, the adsorption capacity at 100 kPa of H_2 decreases from 0.311 mmol/g to 0.194 mmol/g (38 % reduction), while for D_2 it decreases from 0.456 mmol/g to 0.355 mmol/g (22 % reduction). This reduction in adsorption as the temperature is reduced from 159 K to 143 K, suggests the K^+ cations in the K-CHA are starting to block access of H_2 and D_2 molecules to the pores. The results show that between 143 and 178 K, H_2 adsorption is blocked more strongly than D_2, leading to a substantial increase in D_2/H_2 selectivity. The ideal D_2/H_2 selectivity (measured at 100 kPa) rises significantly as the adsorption temperature is reduced, rising from 1.1 at 195 K to a maximum D_2/H_2 selectivity of 1.83 at 143 K. This is a remarkably high D_2/H_2 selectivity for an adsorbent at such a relatively mild temperature. Most adsorbents must be cooled to 77 K or below to achieve similar D_2/H_2 selectivity [32]. The isotherms also suggest that efficient pressure-swing operation would be effective with CHA (further discussed in section 3.6).

Another important observation from Fig. 6(b–e) is that as the temperature is reduced below 159 K the partial desorption isotherm no longer follows the same path as the adsorption isotherm. This adsorption hysteresis is not generally observed for microporous adsorbents like CHA since the standard theory of condensation does not apply in micropores [33]. At higher temperatures (195–178 K) the adsorption/desorption difference becomes negligible which suggests it is linked to the critical admission temperature and therefore evidence of the trapdoor effect in CHA. The hysteresis in CHA is likely caused by energy loss as the gas molecules displace the trapdoor cations. From the literature there are no comparative studies that report hysteresis in the isotherms for CHA. Lozinska et al. [34] reported hysteresis in Zeolite Rho from CO_2 isotherms and they related this to the cation occupancy in the window positions (trapdoor type effect) [10].

3.3. Effect of ion exchange on H_2 and D_2 adsorption – K-CHA and NaK-CHA

It was found that post-synthesis treatment of the K-CHA could significantly alter H_2 and D_2 adsorption despite small changes in the cation composition. Ion exchange treatment of K-CHA in 1 M KCl solution increased the K exchange rate from 97 % to >99 %. It was found from conducting isotherms at 159 K, that this treatment caused H_2 uptake to increase by 50 % and reduced the ideal D_2/H_2 selectivity from 1.49 to 1.18. A similar effect was also observed, when treating the K-CHA with other potassium salt solutions and deionised water. It is thought this post-treatment causes a reduction in the number of hydroxyl groups on the zeolite surface, since the CHA is initially formed in strongly alkaline KOH [35]. Ion exchange treatment of K-CHA using mixed K and Na salts caused the D_2/H_2 selectivity at 159 K to increase from 1.49 to 1.75. The H_2 and D_2 isotherms at 159 K for unmodified K-CHA, ion-exchanged K-CHA and ion-exchanged NaK-CHA are shown in Fig. 7.

3.4. Zeolite 5A H_2/D_2 isotherms at 143–195 K

The H_2 and D_2 adsorption uptake and selectivity of zeolite 5A was measured using isotherm temperatures between 143 and 195 K and the results are shown in Fig. 8. Zeolite 5A has relatively large apertures of 0.5 nm, and so the channels are freely accessible for adsorption of H_2 and D_2 molecules (0.29 nm). The amount of H_2 and D_2 adsorbed increases exponentially with lower temperatures which is the typical trend for

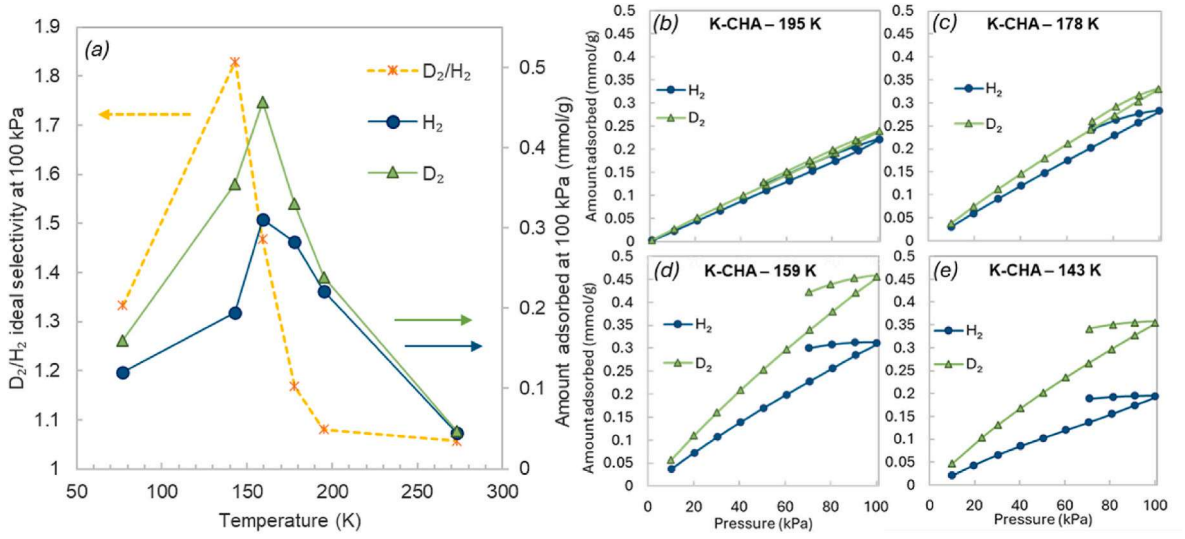

Fig. 6. (a) H_2 and D_2 adsorption and ideal D_2/H_2 selectivity of K-CHA at 100 kPa. Data points from isotherms conducted at different temperatures (b–e) H_2 and D_2 isotherms at temperatures of 195, 178, 159 and 143 K respectively. Isotherm graphs include full adsorption isotherm and partial desorption isotherm.

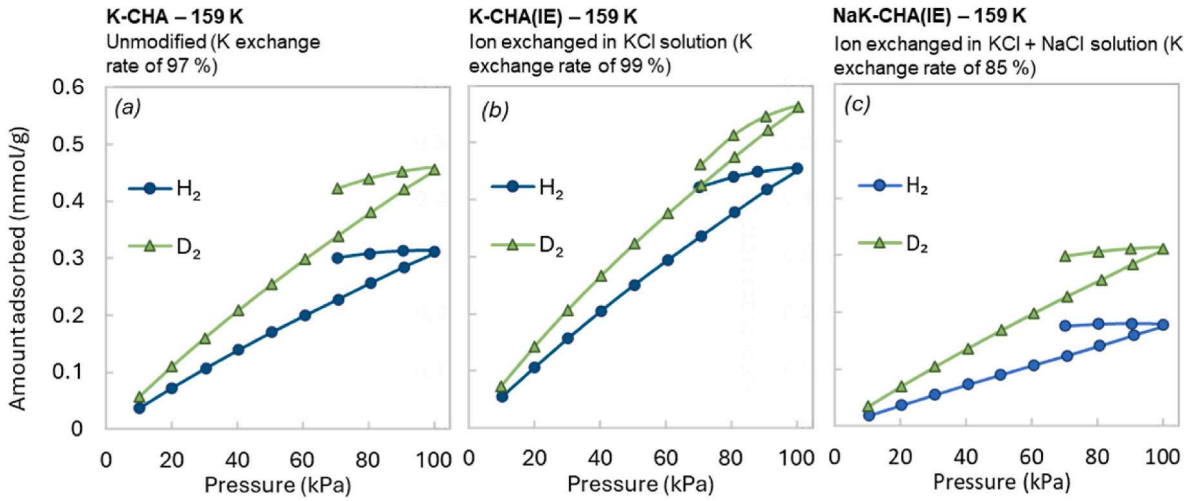

Fig. 7. H_2 and D_2 isotherms at 159 K for CHA with and without ion exchange. Despite minor changes in cation composition, ion exchange treatment increased H_2 uptake by 50 % and reduced D_2/H_2 selectivity. Using mixed Na and K ion exchange, the D_2/H_2 selectivity could be increased.

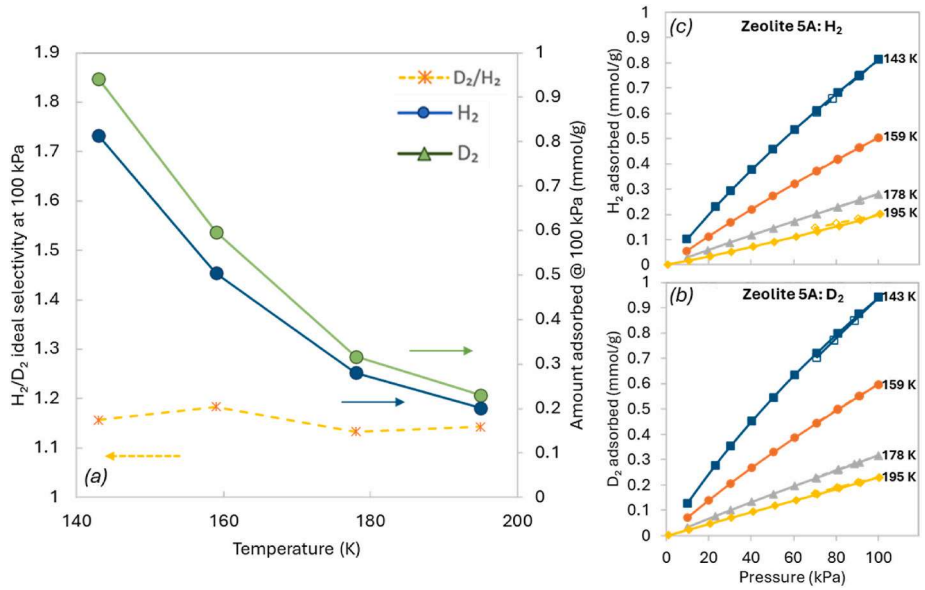

Fig. 8. Effect of temperature on H_2 and D_2 adsorption and ideal D_2/H_2 selectivity of zeolite 5A at 100 kPa. Data points are taken from isotherms conducted at different temperatures.

exothermic physisorption. This is in contrast to K-CHA which contains trapdoor cations that block adsorption at lower temperature. Also, unlike K-CHA, the isotherms show no hysteresis suggesting that there is no trapdoor phenomenon affecting adsorption. The ideal D_2/H_2 selectivity of zeolite 5A of 1.14–1.18 is very low. The data fits well to a linear Van't Hoff plot (shown in supporting information) from which the heat of adsorption at 100 kPa was calculated as 6.35 kJ/mol for H_2 and 6.47 kJ/mol for D_2 on zeolite 5A. This low heat of adsorption is typical for the weak hydrogen interaction with zeolite channels (4–7 kJ/mol for H_2 [36]).

3.5. Zeolite 3A H_2/D_2 isotherms at 143–195 K

The uptake and D_2/H_2 selectivity of zeolite 3A between 143 and 195 K at 100 kPa evaluated from isotherm results are shown in Fig. 9. Zeolite 3A has the same framework structure as zeolite 5A, but the pore aperture is restricted by the presence of K^+ cations. The effective pore aperture is reported to be approximately 0.3 nm which is very close to the size of hydrogen molecules [13].

Zeolite 3A had low uptake of H_2 and D_2 over the whole temperature range. Maximum D_2 uptake of 0.0904 mmol/g was observed at 143 K, only about 10 % of the uptake compared to zeolite 5A. The measured ideal D_2/H_2 selectivity for zeolite 3A reaches a maximum of 1.54 at 159 K. In comparison, zeolite 5A had an ideal D_2/H_2 selectivity of only 1.18 at the same temperature. The higher selectivity of zeolite 3A suggests the K^+ cations in zeolite 3A are able to selectively block H_2 compared to D_2. Comparing to literature data, Kotoh et al. [19] reported maximum D_2 uptake for zeolite 3A of only 0.014 mmol/g which occurred at 170 K and with a D_2/H_2 selectivity of 1.4 [19].

It is generally thought that K^+ cations in the zeolite A framework effectively narrow the pore aperture which limits the molecular size that can access the pore [13,19]. However, H_2 and D_2 have almost identical molecular size and so this would not lead to the observed selectivity. Furthermore, H_2 tends to diffuse faster than D_2 and so this model would produce the opposite isotope selectivity to the one observed. The observed high D_2/H_2 selectivity could suggest a mechanism similar to trapdoor CHA. Zeolite 3A contains K^+ cations in the pore apertures, a feature shared with K-CHA. Furthermore, the D_2/H_2 selectivity of these

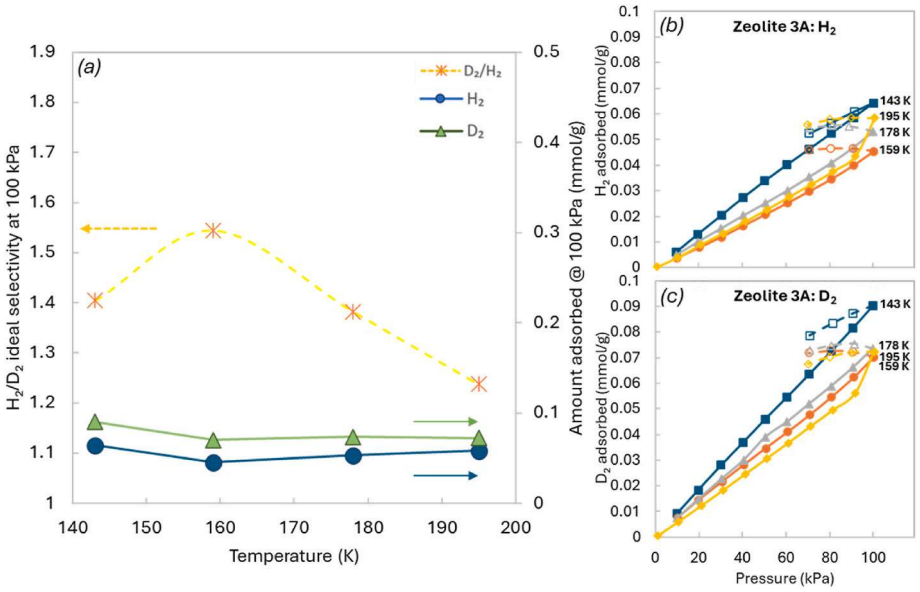

Fig. 9. Zeolite 3A H_2 and D_2 isotherm results conducted at temperatures between 143 and 195 K. (a) D_2/H_2 selectivity and uptake at 100 kPa against temperature; (b) H_2 isotherms; (c) D_2 isotherms.

two adsorbents is remarkably similar, with maximum selectivity occurring in a similar temperature range. This hypothesis of trapdoor behaviour is further supported by the observation of hysteresis in the zeolite 3A isotherms that is not present for zeolite 5A. It is therefore tentatively suggested that the displacement of the K^+ cations in both K-CHA and zeolite 3A is the mechanism that enables H_2 and D_2 molecules to adsorb. However, further evidence will be required to confirm this hypothesis.

3.6. 77 K H_2/D_2 isotherms – MOF-74(Ni), zeolite 5A and HKUST-1

H_2 and D_2 isotherms were measured at 77 K for MOF-74(Ni), HKUST-1 and zeolite 5A and shown in Fig. 10. The ideal D_2/H_2 selectivity was calculated using Ideal Adsorbed Solution Theory (IAST) for a theoretical 50:50 H_2/D_2 mixture.

The linear isotherm plot in Fig. 10(a) shows that MOF-74(Ni) adsorbs significant amounts of H_2 and D_2 at extremely low pressures. This is caused by Ni(II) open metal sites in MOF-74(Ni) which have a very high heat of adsorption for H_2 and D_2 [37]. From the log plot, adsorption begins at around 1 Pa (1×10^{-3} kPa). There are a limited number of open metal sites and once these become saturated, any further H_2 adsorption occurs at much weaker binding sites. The IAST model results estimates a D_2/H_2 selectivity of 3.3 and lower pressures which reduces to 2.1 at higher pressures.

HKUST-1 contains Cu(II) open metal sites which can have a strong interaction with other gases (CO_2 and CH_4) [30,38,39] but from these results it appears that they have a low affinity for H_2. Although HKUST-1 has a weak interaction with H_2, it has very high BET surface area measured to be between 1663 and 2045 m^2/g (see supporting information), and this means that at higher pressures (100 kPa), HKUST-1 can adsorb significant amounts of H_2. However, the D_2/H_2 selectivity is much lower than the other adsorbents tested.

The isotherms in Fig. 10 measured at 77 K, show that zeolite 5A can adsorb H_2 and D_2 at low pressures (0.01–0.1 kPa), with an IAST D_2/H_2 selectivity of 2.4 at 77 K. The IAST model predicts high D_2/H_2 selectivity of 2.4 at low pressure (10^{-3} – 10^{-1} kPa), but above 2 kPa the selectivity

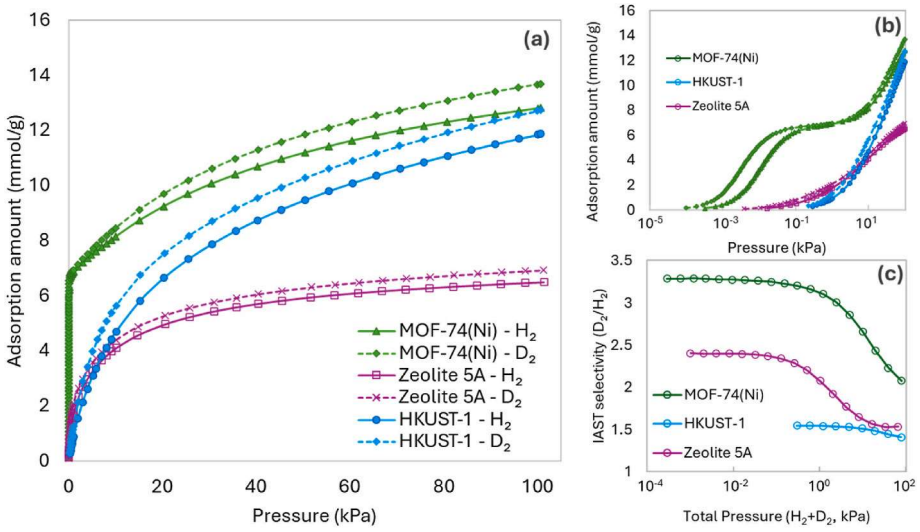

Fig. 10. H_2 and D_2 isotherm results for adsorbents tested at 77 K (MOF-74(Ni), zeolite 5A, HKUST-1). (a) Linear isotherm plots; (b) logarithmic isotherm plots; (c) Ideal D_2/H_2 selectivity calculated using IAST model.

drops to 1.52. At low pressures, H_2 and D_2 essentially only adsorb to the high affinity Ca^{2+} sites in zeolite 5A which have high D_2/H_2 selectivity [18]. At higher pressures, these sites become saturated, and adsorption also occurs on the lower affinity sites, driven by the higher pressures. Since these adsorption sites have lower selectivity, this causes the overall selectivity to drop at higher pressures.

The results show that at 77 K, high affinity adsorption sites such as those present in zeolite 5A and MOF-74(Ni) can achieve high D_2/H_2 selectivity. These adsorbents achieve relatively high D_2 uptake at low temperature compared to the uptake measured by isotherms conducted at 143–195 K. However, high selectivity is only achievable at low pressures (<1 kPa), since at higher pressures adsorption to weaker affinity sites significantly reduces the selectivity. These low pressures will likely be impractical for large scale adsorption, since the column pressure drop can approach the total pressure in the system leading to slow desorption rates. Due to the high affinity for hydrogen isotopes, these adsorbents would need higher temperatures to initiate desorption and would be more challenging to regenerate. Temperature changes can be very slow especially for large columns and are energetically costly at extreme cryogenic temperatures.

In comparison, the isotherm data for K-CHA and NaK-CHA at 143 K and 159 K suggest trapdoor CHA could be pressure regenerated by cycling between 10 and 100 kPa with very little drop in working capacity or selectivity. Note that the D_2/H_2 ideal selectivity of K-CHA of 1.83 at 143 K, was calculated at 100 kPa but rises to 2.26 at 10 kPa. This high D_2/H_2 selectivity of trapdoor CHA over a practical operating pressure regime, make it very promising for large scale isotope separation using energy efficient vacuum pressure-swing operation.

3.7. H_2/D_2 breakthrough testing using whistle gas density sensor

The whistle gas density sensor was calibrated against different D_2 concentrations in H_2 and found to have an almost linear response as shown in Fig. 11(a). The apparent scattering of the raw data points (shown in Fig. 11(b)) is mostly caused by the audio frequency analysis algorithm. The response rate of the sensor was tested using a step change in D_2 concentration (Fig. 11(b)) and demonstrates an almost instantaneous response due to the small volume of the whistle. These characteristics make the whistle gas density sensor well suited for measuring hydrogen isotope breakthrough curves.

The main limitation of the sensor was the minimum required gas flow of 336 ml_n/min which was higher than the flow rate through the experiment. It was found whistle designs with smaller diameter tubes did not significantly reduce the flow requirement. The minimum flow required by a whistle is likely governed by a minimum Reynolds number, since an unstable flow is required to produce a resonating sound. This explains why the minimum flow of H_2 was much higher than when using air, and why using smaller whistle diameters below 1.57 mm did not significantly change the required gas flow. This would be subject to future work but suggests that a whistle design geometry which introduces more turbulence could significantly reduce gas flow requirements making it a viable sensor.

Breakthrough testing was conducted under dynamic flow conditions using a D_2/H_2 binary gas mixture. All adsorbents were tested using two different breakthrough methodologies to compare the kinetics of displacement and competitive D_2/H_2 adsorption. The first is displacement breakthrough, similar to the experiment conducted by Kotoh et al. [40], in which adsorbed H_2 is displaced by D_2 in the test gas. The second experiment is a novel adaption to the standard frontal breakthrough method which was designed specifically to test H_2/D_2 under conditions similar to Vacuum Pressure-Swing Adsorption (VPSA). Instead of using an inert carrier gas as in previous literature studies [25,41,42], adsorption of the D_2/H_2 test gas starts from vacuum pressure. Similar frontal tests have been conducted before on Pd columns [43], but this is the first time it has been applied to porous adsorbents for H_2/D_2 separation. The outlet concentration could only be measured once the column reaches atmospheric pressure. This means the frontal breakthrough will become truncated if the D_2 can reach the column outlet before the H_2 has fully pressurised the system. This reflects the expected column performance under realistic VPSA conditions.

The displacement and frontal breakthrough results for NaK-CHA at 159 K and zeolite 5A at 77 K and 159 K are shown in Fig. 12. NaK-CHA was used for breakthrough tests instead of K-CHA because it exhibited better D_2/H_2 ideal separation as determined from isotherm data.

The whistle gas density sensor is shown to capture the shape of the breakthrough curve in each case. Zeolite 5A at 77 K has the longest breakthrough times due to the higher uptake of this adsorbent at this temperature, despite the higher flow rates of 8.25–24.7 ml_n/(min g) used in these tests compared to 4.19–12.6 ml_n/(min g) for the other tests. For the displacement breakthrough (Fig. 12(a)) a typical symmetrical curve is produced close to an ideal normal distribution. For the frontal experiment (Fig. 12(d)), the curve is not symmetrical because the beginning of the curve is truncated. As previously mentioned, this shows D_2 is reaching the outlet before the column is fully pressurised and

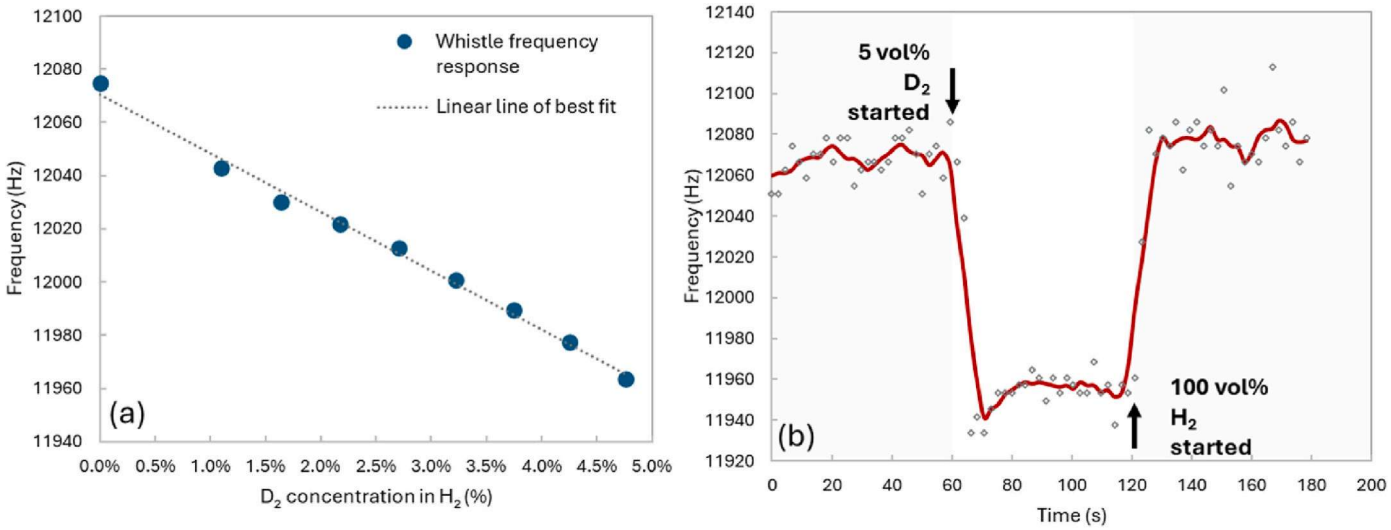

Fig. 11. (a) Frequency response of whistle gas density sensor to D_2 concentration (experimental points shown in blue circle markers and linear line of best fit). For this experiment the H_2 flow was kept constant (360 ml_n/min) with additional D_2 flow added. (b) Time-dependent response of the sensor to a change of 5 % D_2 concentration in H_2. (For interpretation of the references to colour in this figure legend, the reader is referred to the Web version of this article.)

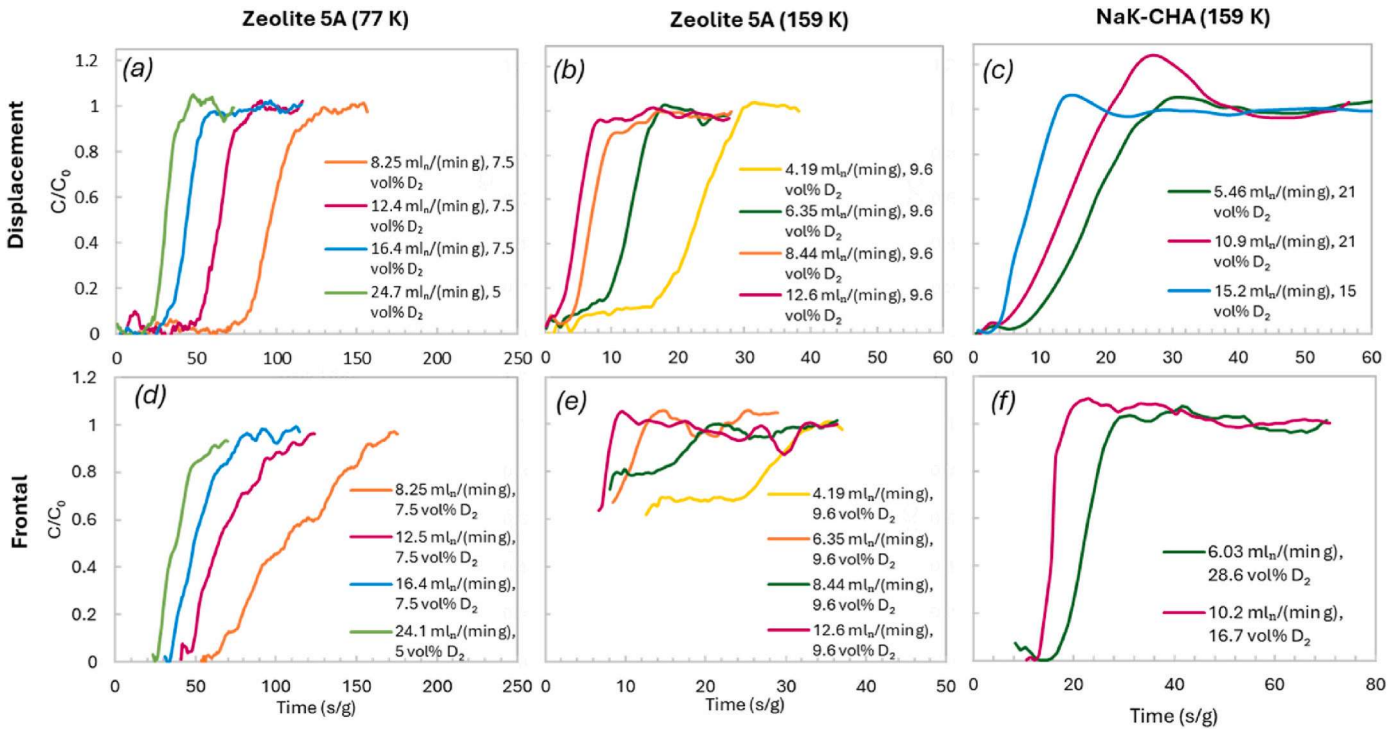

Fig. 12. Mixed H_2/D_2 breakthrough results showing displacement breakthrough results in (a–c) and frontal breakthrough results in (d–f). Results for zeolite 5A at 77 K, zeolite 5A at 159 K and NaK-CHA at 159 K are shown in (a & d), (b & e) and (c & f) respectively. Flow rates as shown in the legend have been standardised against the adsorbent mass. The frontal breakthrough for zeolite 5A at 159 K (shown in (e)) has a truncated breakthrough curve profile with the curve beginning above $C/C_0 = 0.6$. This shows that the column is unable to fully separate the D_2/H_2 mixture. An overshoot (roll-up effect) is observed for NaK-CHA in (c & f).

Table 3
Mean D_2 uptake from displacement and frontal breakthrough experiments. Since the D_2 concentration varied between experiments, assuming uptake is proportional to D_2 concentration, and in the short concentration range, the uptake values have all been standardised at 9.6 vol.% D_2.

Adsorbent	Temp (K)	Standardized D_2 uptake (mmol/g)		% difference in D_2 uptake (frontal – displacement)
		Displacement	Frontal	
Zeolite 5A	77	0.770	0.961	20 %
	159	0.0612	0.0663	8 %
NaK-CHA	159	0.0159	0.0524	70 %

demonstrates the challenge of separating H_2 and D_2 mixtures.

For zeolite 5A at 159 K, the breakthrough time is much shorter than at 77 K indicating lower uptake. The frontal breakthrough curves show that the adsorbent column was unable to fully separate the D_2/H_2 mixture, because breakthrough started at $C/C_0 = 0.6$. Despite the curve beginning at $C/C_0 = 0.6$, the column outlet is closed in the initial portion of the frontal experiment, and so the uptake is still calculated in the same way as shown in Fig. 5. Compared to the displacement experiment, the frontal breakthrough curves exhibit a longer time period between initial breakthrough and equilibrium breakthrough which is also observed to a lesser extent for the 77 K zeolite 5A results. Displacement adsorption causes a self-sharpening mechanism, since any D_2 adsorbed will displace an H_2 molecule, amplifying the concentration gradient caused by adsorption. In frontal breakthrough, D_2 adsorption can occur through displacement, but also competitive adsorption where both H_2 and D_2 is occurring. This reduces the concentration gradient caused by D_2 adsorption and is more important when the selectivity is low, as is the case for zeolite 5A at 159 K.

For NaK-CHA at 159 K, displacement breakthrough, shown in Fig. 12 (c), occurs quickly due to the low uptake of this adsorbent. The frontal breakthrough curve starts at $C/C_0 = 0$ showing that D_2 is being selectivity adsorbed leaving pure H_2 in the outlet gas stream. These results

Table 4
Summary of uptake and D_2/H_2 selectivity as measured by frontal breakthrough results for NaK-CHA at 159 K and zeolite 5A at both 77 K and 159 K and compared to results from isotherm data. For the purposes of comparison, the Isotherm uptake data are adjusted by 15 % to account for 15 wt% inert clay in NaK-CHA and zeolite 5A pellets used in breakthrough results.

Material	Temp (K)	Mean total H_2 & D_2 uptake (mmol/g)		Mean D_2/H_2 selectivity[a]	
		Frontal	Isotherm	Frontal	Isotherm
Zeolite 5A	77	6.2 ± 0.69	5.90[a]	1.7 ± 0.19	1.53
	159	0.58 ± 0.14	0.507[a]	1.25 ± 0.24	1.18
NaK-CHA	159	0.286 ± 0.030	0.265[a]	2.71 ± 0.70	1.75

[a] Actual separation factor and ideal selectivity from isotherm data.

confirm for the first time the ability of the trapdoor effect in NaK-CHA to separate mixtures of hydrogen isotopes at relatively mild cryogenic temperatures. This is in contrast to zeolite 5A which at the same temperature of 159 K, was unable to fully separate the D_2/H_2 mixture. For NaK-CHA at 159 K, the time period between initial breakthrough and equilibrium breakthrough is longest for displacement rather than the frontal experiments. This is the opposite to the two temperature tests for zeolite 5A and is caused by different intra-zeolite diffusion mechanisms. For NaK-CHA, the movement of H_2 molecules through the zeolite pores is restricted by the trapdoor cations. In displacement breakthrough this significantly slows down the H_2 molecules which must leave the zeolite pores for D_2 to adsorb. The self-sharpening displacement mechanism previously described also occurs in NaK-CHA, but is completely offset by the slow diffusion of H_2 in trapdoor CHA. The NaK-CHA displacement breakthrough appear to show a roll-up effect where the D_2 concentration rises above C_0. Roll-up effects are normally caused by a strong adsorbing species which displace a weaker adsorbed species [44], or a difference in the adsorption kinetics between H_2 and D_2.

The mean uptake of D_2 for both the displacement and frontal experiments were calculated and are shown in Table 3. To account for differences in D_2 concentration used in the experiments, the D_2 uptake was standardised to 9.6 vol% D_2, assuming D_2 uptake is proportional to the D_2 concentration given the small concentration range.

For frontal displacement, the mean D_2 uptake is very similar to the equilibrium amount measured from isotherms (see Table 4). However, the mean D_2 uptake from displacement breakthrough is significantly lower than the uptake from frontal breakthrough. This is because in displacement adsorption, the H_2 must diffuse out and this can cause slower adsorption kinetics. For zeolite 5A the uptake difference is more significant at 77 K than at 159 K. This is a similar finding to other authors who found lower temperatures made it more difficult for D_2 to displace H_2 because of the higher heat of adsorption. Fitzgerald et al. [25] found that displacement of H_2 by D_2 on Cu(I)-MFU-4l took much longer as the temperature was reduced from 185 K to 77 K, since H_2 would remain bound to strongly adsorbing sites. The heat of adsorption as measured in section 3.3 for zeolite 5A at 6.35 kJ/mol for H_2 is much lower than Cu(I)-MFU-4l at 32 kJ/mol [25] and so the kinetic hindrance is less. Bezverkhyy et al. [11] also found adsorption of H_2 and D_2 on Na-CHA and Ca-CHA took much longer to reach higher D_2/H_2 selectivity as the temperature was reduced from 77 K to 38 K.

NaK-CHA has the most significant difference in uptake with 70 % lower D_2 uptake from displacement breakthrough compared to frontal breakthrough. In displacement adsorption, the trapdoor effect is expected to significantly slow down H_2 molecules which must diffuse outwards through the CHA trapdoor cations before D_2 can adsorb. Since H_2 molecules cannot diffuse out through the trapdoor quickly enough, this prevents D_2 from diffusing in and adsorbing. By contrast, in frontal breakthrough, the D_2 can interact with the trapdoor cation without the need for H_2 to exit from the CHA pores. This allows the D_2 molecules to pass more freely through the trapdoor windows, leading to close to equilibrium uptake. This is an important finding that shows trapdoor CHA performs best in frontal adsorption applications such as PSA, but is poorly suited to displacement chromatography applications.

Table 4 presents the mean total uptake (H_2 + D_2) and separation factor from the frontal breakthrough experiments and from the adsorption isotherm experiments in section 3.2–3.5. In all cases, the uptake from the frontal breakthrough experiments is between 5 and 14 % greater than the isotherm uptake. It is thought this small difference follows from experimental error in the breakthrough experiment and reflects the challenge of breakthrough experimentation with hydrogen isotopologues given their low uptake. The zeolite 5A data at 77 K is in good agreement with literature data tested under similar conditions. Kotoh et al. tested zeolite 5A at 77 K under mixed isotope conditions [45] and reported a separation factor of 2.0 at 1 bar. This agreement with the literature and isotherm data helps to confirm the effectiveness of the frontal breakthrough method in measuring the D_2/H_2 selectivity.

For NaK-CHA at 159 K, the mean D_2/H_2 separation factor of 2.71 ± 0.70 from the frontal breakthrough results is significantly higher than the D_2/H_2 selectivity of 1.75 predicted by the isotherm data. This was an expected result because individual gas isotherm data cannot fully replicate the behaviour and selectivity of mixed gas systems [44]. Note that the error from the NaK-CHA breakthrough experiment is relatively large due to the low flow rates required by the experiment. The D_2 uptake for NaK-CHA of 0.286 mmol/g (see Table 4) is much lower than the other adsorbents with a D_2 uptake for MOF-74(Ni) of 13.7 mmol/g at 77 K (see Fig. 10) and for zeolite 5A of 6.2 mmol/g. Also other adsorbents tested in the literature such as metal doped zeolites [10] and open metal site MOFs [17,46] can achieve higher D_2/H_2 selectivity at similar temperatures to CHA. However, these adsorbents either have very high adsorption enthalpy or operate at <77 K temperatures making it difficult to desorb the H_2 and D_2 after each cycle requiring temperature-swing operation. In contrast, CHA has a low adsorption enthalpy and operates at high temperatures, meaning pressure-swing operation could be effective at desorbing the gases. Pressure-swing cycles can be very fast since the column doesn't need heating or cooling and could potentially operate at higher pressures. Both these factors would offset the low uptake of CHA and enable higher throughputs with lower energy use and mild operating conditions as required for future fusion applications.

4. Conclusion

Trapdoor chabazite was shown to have a high hydrogen isotope selectivity at temperatures much higher than other adsorbents using both single gas isotherms and mixed gas breakthrough tests. Evidence of a cation displacement mechanism in zeolite 3A is also reported for the first time. The ideal D_2/H_2 selectivity of K-CHA is highly temperature sensitive, with almost no selectivity at 195 K, but rising to 1.75 at 143 K as the critical admission temperature is reached and H_2 starts to be blocked. A hysteresis effect is reported in trapdoor CHA and zeolite 3A for the first time which only occurs between 143 and 178 K. The favourable adsorption equilibria of trapdoor CHA suggest that pressure-driven desorption could be used enabling the adsorbent to be rapidly cycled even in large scale applications.

A bespoke breakthrough setup using a novel online whistle gas density sensor was successfully used to test dynamic H_2/D_2 adsorption in NaK-CHA at 159 K and zeolite 5A at 77 K and 159 K. The detection system was able to replace more complex mass spectrometry and achieve real-time isotope measurements in an inexpensive setup. Future work could investigate different whistle geometries to reduce the minimum gas requirements which was its main limitation. Using the breakthrough apparatus, the D_2/H_2 separation factor of NaK-CHA was measured under mixed gas flow conditions to be approximately 2.71 ± 0.70 at 159 K, 1 bar. In contrast to zeolite 5A, NaK-CHA achieved better isotope separation in frontal breakthrough than displacement breakthrough showing trapdoor CHA is more well suited to PSA operation rather than displacement chromatography. These results demonstrate that high hydrogen isotope selectivity is achievable at practical mild cryogenic temperatures in trapdoor adsorbents. Trapdoor CHA has the potential for efficient large scale isotope separation with low tritium inventory, addressing one of the key challenges facing the realisation of commercial fusion plants.

CRediT authorship contribution statement

Lawrence Shere: Writing – review & editing, Writing – original draft, Visualization, Validation, Software, Methodology, Investigation, Formal analysis, Data curation, Conceptualization. **Niklas Beere:** Validation, Investigation, Formal analysis. **Rosemary Brown:** Writing – review & editing, Supervision, Resources, Project administration. **Rachel Lawless:** Supervision, Project administration, Funding acquisition. **Timothy J. Mays:** Writing – review & editing, Supervision, Project administration, Funding acquisition. **Semali P. Perera:** Writing –

review & editing, Supervision, Resources, Methodology, Conceptualization. **Alfred K. Hill:** Writing – review & editing, Supervision, Project administration, Funding acquisition, Conceptualization.

Declaration of competing interest

The authors declare that they have no known competing financial interests or personal relationships that could have appeared to influence the work reported in this paper.

Acknowledgments

This research is supported by the UK Atomic Energy Authority (UKAEA) and the H3AT division.

Appendix A. Supplementary data

Supplementary data to this article can be found online at https://doi.org/10.1016/j.ijhydene.2025.152753.

References

[1] Association WN. Nuclear fusion power [cited 04/01/21]. Available from: https://www.world-nuclear.org/information-library/current-and-future-generation/nuclear-fusion-power.aspx; 2020.
[2] Chapman IT, Morris AW. UKAEA capabilities to address the challenges on the path to delivering fusion power. Philos Trans A Math Phys Eng Sci 2019;377(2141):20170436.
[3] Lawless R, Butler B, Hollingsworth A, Camp P, Shaw R. Tritium plant technology development for a DEMO power plant. Fusion Sci Technol 2017;71(4):679–86.
[4] Shaw RCR, Butler B. Applicability of a cryogenic distillation system for D-T isotope rebalancing and protium removal in a DEMO power plant. Fusion Eng Des 2019;141:59–67.
[5] Day C, Battes K, Butler B, Davies S, Farina L, Frattolillo A, George R, Giegerich T, Hanke S, Härtl T, Igitkhanov Y, Jackson T, Jayasekera N, Kathage Y, Lang PT, Lawless R, Luo X, Neugebauer C, Ploeckl B, Santucci A, Schwenzer J, Teichmann T, Tijssen T, Tosti S, Varoutis S, Cortes AV. The pre-concept design of the DEMO tritium, matter injection and vacuum systems. Fusion Eng Des 2022;179:113139.
[6] Bainbridge N, Bell AC, Brennan PD, Knipe S, Lässer R, Stagg R. Operational experience with the JET AGHS cryodistillation system during and after DTE1. Fusion Eng Des 1999;47(2):321–32.
[7] Roder HM, Childs GE, McCarty RD, Angerhofer PE. Survey of the properties of the hydrogen isotopes below their critical temperatures. United States: National Bureau of Standards; 1973.
[8] Kim JY, Oh H, Moon HR. Hydrogen isotope separation in confined nanospaces: carbons, zeolites, metal–organic frameworks, and covalent organic frameworks. Adv Mater 2019;31(20):1805293.
[9] Weinrauch I, Savchenko I, Denysenko D, Souliou SM, Kim HH, Le Tacon M, Daemen LL, Cheng Y, Mavrandonakis A, Ramirez-Cuesta AJ, Volkmer D, Schütz G, Hirscher M, Heine T. Capture of heavy hydrogen isotopes in a metal-organic framework with active Cu(I) sites. Nat Commun 2017;8(1):14496.
[10] Zhang L, Wulf T, Baum F, Schmidt W, Heine T, Hirscher M. Chemical affinity of Ag-Exchanged zeolites for efficient hydrogen isotope separation. Inorg Chem 2022;61(25):9413–20.
[11] Bezverkhyy I, Boyer V, Cabaud C, Bellat J-P. High efficiency of Na- and Ca-Exchanged chabazites in D2/H2 separation by Quantum sieving. ACS Appl Mater Interfaces 2022;14(47):52738–44.
[12] Shang J, Li G, Singh R, Gu Q, Nairn KM, Bastow TJ, Medhekar N, Doherty CM, Hill AJ, Liu JZ, Webley PA. Discriminative separation of gases by a "Molecular Trapdoor" mechanism in chabazite zeolites. J Am Chem Soc 2012;134(46):19246–53.
[13] Kulprathipanja S. Zeolites in industrial separation and catalysis. John Wiley & Sons; 2010.
[14] Li G, Shang J, Gu Q, Awati RV, Jensen N, Grant A, Zhang X, Sholl DS, Liu JZ, Webley PA, May EF. Temperature-regulated guest admission and release in microporous materials. Nat Commun 2017;8(1):15777.
[15] Physick AJW, Wales DJ, Owens SHR, Shang J, Webley PA, Mays TJ, Ting VP. Novel low energy hydrogen–deuterium isotope breakthrough separation using a trapdoor zeolite. Chem Eng J 2016;288:161–8.
[16] Taguchi A, Hamashima H, Nakamori T, Yoneyama Y. Thermal adsorption spectroscopy of hydrogen isotopes from CHA-type zeolites. Fusion Sci Technol 2024;80:359–64.
[17] FitzGerald SA, Pierce CJ, Rowsell JLC, Bloch ED, Mason JA. Highly selective quantum sieving of D2 from H2 by a metal–organic framework as determined by gas manometry and infrared spectroscopy. J Am Chem Soc 2013;135(25):9458–64.
[18] Giraudet M, Bezverkhyy I, Weber G, Dirand C, Macaud M, Bellat J-P. D2/H2 adsorption selectivity on FAU zeolites at 77.4 K: influence of Si/Al ratio and cationic composition. Microporous Mesoporous Mater 2018;270:211–9.
[19] Kotoh K, Kimura K, Nakamura Y, Kudo K. Hydrogen isotope separation using molecular sieve of synthetic zeolite 3A. Fusion Sci Technol 2008;54(2):419–22.
[20] Lin C-H, Lin C-H, Li Y-S, He Y-S. Development and application of a milli-whistle for use in gas chromatography detection. Anal Chem 2010;82(17):7467–71.
[21] Walker RJ. Sonic standing wave gas density monitor. In: Fast RW, editor. Advances in cryogenic engineering. Boston, MA: Springer US; 1988. p. 1081–7.
[22] Cadot S, Veyre L, Luneau D, Farrusseng D, Alessandra Quadrelli E. A water-based and high space-time yield synthetic route to MOF Ni2(dhtp) and its linker 2,5-dihydroxyterephthalic acid. J Mater Chem A 2014;2(42):17757–63.
[23] Schlichte K, Kratzke T, Kaskel S. Improved synthesis, thermal stability and catalytic properties of the metal-organic framework compound Cu3(BTC)2. Microporous Mesoporous Mater 2004;73(1):81–8.
[24] Rouquerol J, Rouquerol F, Sing K. Adsorption by powders and porous solids : principles, methodology and applications. San Diego, United Kingdom. Elsevier Science & Technology; 1998.
[25] FitzGerald SA, Mukasa D, Rigdon KH, Zhang N, Barnett BR. Hydrogen isotope separation within the metal–organic framework Cu(I)-MFU-4l. J Phys Chem C 2019;123(50):30427–33.
[26] Baerlocher C, McCusker LB. Database of zeolite structures [Internet] [cited 09/09/2023]. Available from: http://www.iza-structure.org/databases/; 2017.
[27] Shang J, Li G, Singh R, Xiao P, Liu JZ, Webley PA. Determination of composition range for "Molecular Trapdoor" effect in chabazite zeolite. J Phys Chem C 2013;117(24):12841–7.
[28] Chen C, Feng X, Zhu Q, Dong R, Yang R, Cheng Y, He C. Microwave-assisted rapid synthesis of well-shaped MOF-74 (Ni) for CO2 efficient capture. Inorg Chem 2019;58(4):2717–28.
[29] Kim JY, Balderas-Xicohténcatl R, Zhang L, Kang SG, Hirscher M, Oh H, Moon HR. Exploiting diffusion barrier and chemical affinity of metal–organic frameworks for efficient hydrogen isotope separation. J Am Chem Soc 2017;139(42):15135–41.
[30] Moellmer J, Moeller A, Dreisbach F, Glaeser R, Staudt R. High pressure adsorption of hydrogen, nitrogen, carbon dioxide and methane on the metal–organic framework HKUST-1. Microporous Mesoporous Mater 2011;138(1):140–8.
[31] Hartmann M, Kunz S, Himsl D, Tangermann O, Ernst S, Wagener A. Adsorptive separation of isobutene and isobutane on Cu3(BTC)2. Langmuir 2008;24(16):8634–42.
[32] Beenakker JJM, Borman VD, Krylov SY. Molecular transport in subnanometer pores: zero-point energy, reduced dimensionality and quantum sieving. Chem Phys Lett 1995;232(4):379–82.
[33] Donohue MD, Aranovich GL. Adsorption hysteresis in porous solids. J Colloid Interface Sci 1998;205(1):121–30.
[34] Lozinska MM, Mangano E, Mowat JPS, Shepherd AM, Howe RF, Thompson SP, Parker JE, Brandani S, Wright PA. Understanding carbon dioxide adsorption on univalent cation forms of the flexible zeolite rho at conditions relevant to carbon capture from flue gases. J Am Chem Soc 2012;134(42):17628–42.
[35] Chu P, Dwyer FG. The deammoniation reaction of ammonium X zeolite. J Catal 1980;61(2):454–60.
[36] Knight EW, Gillespie AK, Prosniewski MJ, Stalla D, Dohnke E, Rash TA, Pfeifer P, Wexler C. Determination of the enthalpy of adsorption of hydrogen in activated carbon at room temperature. Int J Hydrogen Energy 2020;45(31):15541–52.
[37] FitzGerald SA, Burkholder B, Friedman M, Hopkins JB, Pierce CJ, Schloss JM, Thompson B, Rowsell JL. Metal-specific interactions of H2 adsorbed within isostructural metal-organic frameworks. J Am Chem Soc 2011;133(50):20310–8.
[38] Chong KC, Lai SO, Mah SK, Thiam HS, Chong WC, Shuit SH, Lee SS, Chong WE. A review of HKUST-1 metal-organic frameworks in gas adsorption. IOP Conf Ser Earth Environ Sci 2023;1135(1):012030.
[39] Liu J, Culp JT, Natesakhawat S, Bockrath BC, Zande B, Sankar SG, Garberoglio G, Johnson JK. Experimental and theoretical studies of gas adsorption in Cu3(BTC)2: an effective activation procedure. J Phys Chem C 2007;111(26):9305–13.
[40] Kotoh K, Moriyama S-t, Takashima S, Takahashi K. Breakthrough curves of non-trace H2–D2 mixture replacement adsorption with SZ-13X packed column at 77.4K. Fusion Eng Des 2013;88(9):2223–7.
[41] Wu F, Li L, Tan Y, El-Sayed E-SM, Yuan D. The competitive and synergistic effect between adsorption enthalpy and capacity in D2/H2 separation of M2(m-dobdc) frameworks. Chin Chem Lett 2021;32(11):3562–5.
[42] Si Y, He X, Jiang J, Duan Z, Wang W, Yuan D. Highly effective H2/D2 separation in a stable Cu-based metal-organic framework. Nano Res 2021;14(2):518–25.
[43] Fukada S, Fujiwara H. Comparison of chromatographic methods for hydrogen isotope separation by Pd beds. J Chromatogr A 2000;898(1):125–31.
[44] Thomas WJ, Crittenden B. Adsorption technology and design. Oxford: Buttenworth-Heinemann; 1998.
[45] Kotoh K, Kudo K. Multi-component adsorption behavior of hydrogen isotopes on zeolite 5A and 13X at 77.4 K. Fusion Sci Technol 2005;48(1):148–51.
[46] Teufel J, Oh H, Hirscher M, Wahiduzzaman M, Zhechkov L, Kuc A, Heine T, Denysenko D, Volkmer D. MFU-4 – a metal-organic framework for highly effective H2/D2 separation. Adv Mater 2013;25(4):635–9.